Available online at www.sciencedirect.com
ScienceDirect
Journal of Solid State Chemistry 180 (2007) 2541–2549
JOURNAL OF SOLID STATE CHEMISTRY
www.elsevier.com/locate/jssc

Line patterning of $(Sr,Ba)Nb_2O_6$ crystals in borate glasses by transition metal atom heat processing

M. Sato, T. Honma, Y. Benino, T. Komatsu*

Department of Materials Science and Technology, Nagaoka University of Technology, 1603-1 Kamitomioka-cho, Nagaoka 940-2188, Japan

Received 3 April 2007; received in revised form 12 June 2007; accepted 22 June 2007
Available online 7 July 2007

Abstract

Some NiO-doped Bi_2O_3,La_2O_3–SrO–BaO–Nb_2O_5–B_2O_3 glasses giving the formation of strontium barium niobate $Sr_{0.5}Ba_{0.5}Nb_2O_6$ (SBN) crystals with a tetragonal tungsten–bronze structure through conventional crystallization in an electric furnace have been developed, and SBN crystal lines have been patterned on the glass surface by heat-assisted (250–300 °C) laser irradiation and scanning of continuous-wave Nd:YAG laser (wavelength: 1064 nm). The surface morphology and the quality of SBN crystal lines are examined from measurements of confocal scanning laser micrographs and polarized micro-Raman scattering spectra. The surface morphology of SBN crystal lines changes from periodic bump structures to homogeneous structures, depending on laser scanning conditions. It is suggested that the line patterned at the laser irradiation condition of laser power $P = 1$ W and of laser scanning speed $S = 1$ μm/s in $2NiO–4La_2O_3–16SrO–16BaO–32Nb_2O_5–30B_2O_3$ glass has a possibility of the orientation of SBN crystals along the laser scanning direction. The present study demonstrates that the transition metal atom heat processing (i.e., a combination of cw Nd:YAG laser and Ni^{2+} ions) is a novel technique for spatially selected crystallization of SBN crystals in glass.

Keywords: Glass; Crystal line; Laser irradiation; Polarized Raman scattering spectra; $(Sr,Ba)Nb_2O_6$

1. Introduction

Strontium barium niobates, $Sr_xBa_{1-x}Nb_2O_6$ (hereafter referred to as SBN) with $0.25 \leqslant x \leqslant 0.75$, are well-known crystals with a tetragonal tungsten–bronze structure and possess various excellent ferroelectric and nonlinear optical properties such as extremely large electro-optic coefficients [1–3]. Numerous studies on fabrication and characterization of SBN crystals have been, therefore, reported by many researchers so far. As the growth of bulk SBN single crystals is difficult [4], it is important to develop fabrication techniques for SBN crystals with high crystal qualities and performances. For instance, it has been strongly desired to develop thin films or transparent ceramics consisting of highly oriented SBN crystals.

Crystallization of glass is a method for fabrication of transparent and dense condensed materials with desired shapes, nanostructures and highly oriented crystals [5–8]. It has been reported that some glasses in the systems of SrO–BaO–Nb_2O_5–TeO_2 and SrO–BaO–Nb_2O_5–SiO_2 give SBN ferroelectrics with a tetragonal tungsten–bronze structure by using a conventional crystallization technique in an electric furnace [9,10]. There has been, however, no report on the successful control of the orientation of SBN crystals in crystallized glasses. On the other hand, recently, laser irradiation to glass has received much attention, because it has been recognized that spatially selected structural modification is realized in glass by using laser irradiation technique [11–13]. It is of particular interest to develop laser irradiation techniques being possible to design SBN crystals in a desired part of glass.

The present authors' group [14–17] proposed two laser irradiation techniques for the patterning of crystal dots and lines on the glass surface, i.e., rare-earth atom heat (REAH) processing and transition metal atom heat (TMAH) processing. In these processing methods, continuous-wave (cw) Nd:YAG lasers with a wavelength of $\lambda = 1064$ nm are irradiated to glasses with some amounts of rare-earth (RE) ions such as Sm^{3+} or Dy^{3+} and

*Corresponding author. Fax: +81 258 47 9300.
E-mail address: komatsu@mst.nagaokaut.ac.jp (T. Komatsu).

0022-4596/$ - see front matter © 2007 Elsevier Inc. All rights reserved.
doi:10.1016/j.jssc.2007.06.026

transition metal (TM) ions such as Ni^{2+} or Fe^{2+}. Irradiated lasers are absorbed by RE ions in glass through *f–f* transitions and TM ions through *d–d* transitions, and absorbed energies are converted to thermal energies through non-radiative relaxation process (electron–phonon couplings). And thus surroundings of RE or TM ions are heated locally, consequently inducing effectively structural modifications such as refractive index change or crystallization in glass. The present authors' group proposed to call these techniques "REAH processing" and "TMAH processing", respectively [15–17]. Using these techniques, the present authors' group has succeeded in writing crystal lines consisting of nonlinear or ferroelectric crystals such as β-BaB_2O_4, β′-$Sm_2(MoO_4)_3$, and $Ba_2TiGe_2O_8$ [15–22]. Very recently, Gupta et al. [23] reported the formation of $Nd_xLa_{1-x}BGeO_5$ crystal dots and lines on the surface of $Nd_{0.2}La_{0.8}BGeO_5$ glass by irradiations of cw titanium–sapphire laser with $\lambda = 800$ nm, in which the absorption of laser light with $\lambda = 800$ nm by Nd^{3+} and consequent non-radiative relaxation process have been applied.

In this paper, we focus our attention on the patterning of SBN crystal lines on the glass surface by using a technique of TMAH processing developed by our research group. In previous paper [18], the formation of $Sr_{0.5}Ba_{0.5}Nb_2O_6$ ferroelectrics was confirmed in Sm_2O_3–SrO–BaO–Nb_2O_5–B_2O_3 glasses by using REAH processing, but the control of crystallization and morphology was not difficult, and homogeneous SBN crystal lines were not patterned. In this study, therefore, we apply another laser-induced crystallization technique of TMAH processing to glass. There has been no report on the crystallization of SBN crystals by using laser irradiation except our previous study [18]. We also discuss the mechanism of laser-induced crystallization in glass.

2. Experimental

In the previous paper [18] on the crystallization of $Sr_{0.5}Ba_{0.5}Nb_2O_6$ ferroelectrics, the glasses with various compositions in the system of Sm_2O_3–SrO–BaO–Nb_2O_5–B_2O_3 were developed and used, where B_2O_3 was added to form the glassy state in melt-quenched samples. For instance, $5Sm_2O_3$–11.25SrO–11.25BaO–$22.5Nb_2O_5$–$50B_2O_3$ (mol%) and $10Sm_2O_3$–10SrO–10BaO–$20Nb_2O_5$–$50B_2O_3$ (mol%) glasses were found to form ferroelectric $Sr_{0.5}Ba_{0.5}Nb_2O_6$ crystals through heat treatments in an electric furnace or cw Nd:YAG laser irradiation (a wavelength of $\lambda = 1064$ nm). In the laser-induced crystallization of TMAH processing [17], we need to include small amounts of TM ions such as Ni^{2+} and Fe^{2+} in glass instead of Sm^{3+} or Dy^{3+}, and Ni^{2+} was selected in this study. The glass systems examined in the present study are NiO–Bi_2O_3 (or La_2O_3)–SrO–BaO–Nb_2O_5–B_2O_3, and the glass compositions are shown in Table 1. It should be pointed out that the glasses have the composition of $Sr_{0.5}Ba_{0.5}Nb_2O_6$ for SrO, BaO and Nb_2O_5 components. Bi_2O_3 and La_2O_3 were added to improve the glass-forming ability in the SrO–BaO–Nb_2O_5–B_2O_3 system.

The glasses were prepared using a conventional melt quenching method. Commercial powders of reagent grade NiO, Bi_2O_3, La_2O_3, $SrCO_3$, $BaCO_3$, Nb_2O_5, B_2O_3 were mixed and melted in a platinum crucible at 1400 °C for 1 h in an electric furnace. A small amount (0.2 mol%) of Sb_2O_3 was added to decrease the degree of brown coloration due to the valence change of Bi ions during melting. The melts were poured onto an iron plate and pressed to a thickness of ~1.5 mm with another iron plate. The glass transition, T_g, and crystallization peak, T_p, temperatures were determined using differential thermal analyses (DTA) at a heating rate of 10 K/min. Optical absorption spectra were measured in the wavelength range of 250–2000 nm using a spectrometer.

The glasses were mechanically polished to a mirror finish with CeO_2 powders. A cw Nd:YAG laser with $\lambda = 1064$ nm was irradiated to the glass surface using objective lens (20 or 60 magnification). The glasses were put on the stage heated at 250 or 300 °C and mechanically moved during laser irradiation to construct crystal lines. The laser power was fixed to $P = 1$ W, and the translation speed of the sample stage was changed from $S = 0.5$ to 20 μm/s. The morphology of crystal lines was observed with polarization optical (OLYMPUS-BX51) and confocal scanning laser (OLYMPUS-OLS3000) microscopes, and the crystalline phase was examined from X-ray diffraction (XRD) analyses (Cu*K*α radiation) at room temperature and micro-Raman scattering spectra (Tokyo Instruments Co., Nanofinder; Ar^+ laser 488 nm).

3. Results and discussion

3.1. Thermal and optical properties of glasses

The glasses prepared in this study are designated here as Glass A for 2NiO–$4Bi_2O_3$–11.25SrO–11.25BaO–22.5 Nb_2O_5–$49B_2O_3$, Glass B for 2NiO–$4Bi_2O_3$–16SrO–16BaO–

Table 1
Glass compositions, glass transition temperature, T_g, crystallization peak, T_p, temperatures, and optical absorption coefficients, α, at the wavelength of $\lambda = 1064$ nm in the glasses examined in this study

Sample no.	Glass composition (mol%)	T_g (°C)	T_p (°C)	α (cm^{-1})
Glass A	2NiO–$4Bi_2O_3$–11.25SrO–11.25BaO–$22.5Nb_2O_5$–$49B_2O_3$	555	638	3.9
Glass B	2NiO–$4Bi_2O_3$–16SrO–16BaO–$32Nb_2O_5$–$30B_2O_3$	560	673	3.7
Glass C	2NiO–$4La_2O_3$–16SrO–16BaO–$32Nb_2O_5$–$30B_2O_3$	611	723	3.3

$32Nb_2O_5$–$30B_2O_3$, and Glass C for $2NiO$–$4La_2O_3$–$16SrO$–$16BaO$–$32Nb_2O_5$–$30B_2O_3$.

All melt-quenched samples showed optically clear transparencies. The glassy state of the melt-quenched samples was examined by using XRD analyses, indicating only broad halo patterns being typical for glass materials. All three samples prepared in this study are, therefore, confirmed to be glass. It should be pointed out that Glass B and Glass C have a relatively small amount of B_2O_3, i.e., 30 mol% and thus have a large amount of SrO, BaO, and Nb_2O_5 components. It is considered that a small addition of Bi_2O_3 or La_2O_3 is enhancing largely the glass forming ability.

The DTA patterns for the glasses are shown in Fig. 1. The peaks due to the glass transition and crystallization are clearly detected. In particular, only one crystallization peak is observed in each glass, implying the formation of one crystalline phase during crystallization. The values of glass transition and crystallization peak temperatures for the glasses are given in Table 1, i.e., $T_g = 555\,^{\circ}C$ and $T_p = 638\,^{\circ}C$ for Glass A, $T_g = 560\,^{\circ}C$ and $T_p = 673\,^{\circ}C$ for Glass B, and $T_g = 611\,^{\circ}C$ and $T_p = 723\,^{\circ}C$ for Glass C. The addition of La_2O_3 tends to increase the glass transition and crystallization peak temperatures. The glasses were heat-treated at T_p for 3 h in an electric furnace, and crystalline phases present in the heat-treated samples were examined by XRD analyses. As an example, the XRD pattern for Glass A is shown in Fig. 2. All peaks are assigned to $Sr_{0.5}Ba_{0.5}Nb_2O_6$ crystal (JCPDS 39-0265). For other Glass B and Glass C, the crystallization of $Sr_{0.5}Ba_{0.5}Nb_2O_6$ was confirmed from XRD patterns. It should be pointed out that the Sr/Ba ratio in $Sr_xBa_{1-x}Nb_2O_6$ crystals formed in the crystallized glasses is consistent with the Sr/Ba ratio in the precursor glasses. Similar results, i.e., the formation of $Sr_{0.5}Ba_{0.5}Nb_2O_6$ crystals, have been observed in the crystallization of Sm_2O_3–SrO–BaO–Nb_2O_5–B_2O_3 glasses [18].

The optical absorption spectrum at room temperature for Glass A is shown in Fig. 3, as an example. The absorption band with a strong intensity at ~430 nm and a broad band centered at ~850 nm are observed. These peaks are typical for Ni^{2+} in glass [24–27]. It is well known that the coordination of Ni^{2+} is very sensitive to their ligand field environments, i.e., ionic-bonded octahedral coordination in acidic (low optical basicity) glasses and covalent-bonded tetrahedral coordination in high basicity glasses [25], consequently giving the change in the ratio of the amount of octahedral and tetrahedral coordinated Ni^{2+} in glass [26]. The spectrum shown in Fig. 3, however, suggests that Ni^{2+} in the glasses prepared in this study have mainly octahedral coordination environments, because the peaks at around 430 and 850 nm are typical for octahedral coordinated Ni^{2+} in glass [27]. The absorption coefficient, α, at 1064 nm is $\alpha = 3.9\,cm^{-1}$ for Glass A. Similar optical absorption spectra were obtained for other glasses, giving the values of $\alpha = 3.7\,cm^{-1}$ for Glass B and $\alpha = 3.3\,cm^{-1}$ for Glass C. These absorption coefficients are comparable to those for Sm_2O_3-doped glasses, e.g., $\alpha = 4.5\,cm^{-1}$ for $10Sm_2O_3$–$10SrO$–$10BaO$–$20Nb_2O_5$–$50B_2O_3$ glass [18], and it is expected that Nd:YAG laser-irradiated spots in these

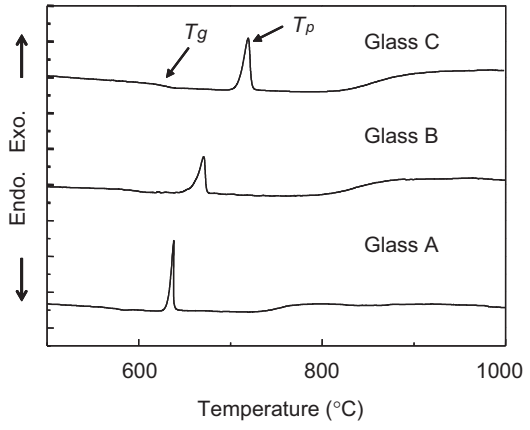

Fig. 1. DTA patterns for Glass A, Glass B, and Glass C. T_g and T_p are the glass transition and crystallization peak temperatures, respectively. The heating rate was 10 K/min.

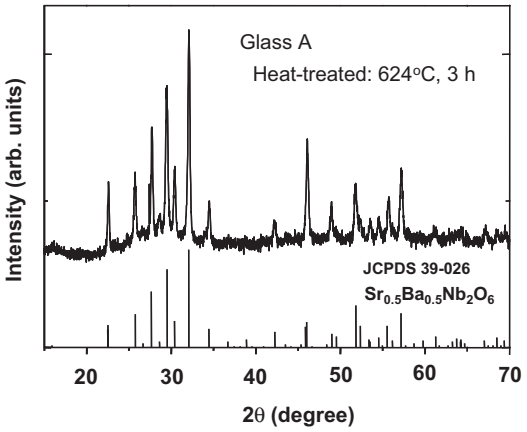

Fig. 2. XRD pattern for the crystallized glass obtained by heat treatment at 624 °C for 3 h in Glass A. All peaks are assigned to $Sr_{0.5}Ba_{0.5}Nb_2O_6$ crystals.

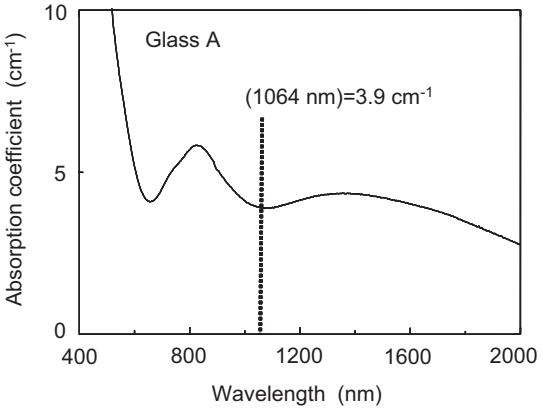

Fig. 3. Optical absorption spectrum at room temperature for Glass A. The absorption coefficient at 1064 nm is $3.9\,cm^{-1}$.

glasses would be heated as similar to the case of Sm_2O_3-doped glasses.

3.2. Patterning of SBN crystal lines by laser irradiation

As stated in the above section, it was clarified that SBN crystals are formed as the initial crystalline phase in the crystallization of NiO-doped Bi_2O_3 or La_2O_3–SrO–BaO–Nb_2O_5–B_2O_3 glasses. We tried to write lines consisting of SBN crystals on the glass surface by irradiations of cw Nd:YAG laser. In the laser irradiation experiments, a heat-assisted method was applied, in which glass samples were put on the sample stage heated at 250 or 300 °C during laser irradiation. The temperatures of 250 and 300 °C are far below from the glass transition temperatures (555–611 °C) of the glasses. Without a heat-assisted method, it was difficult to induce crystallization in the glasses by using the laser irradiation condition of laser power $P = 1$ W. A heat-assisted method has also an effect in the depression of sudden sample's breaks due to thermal shock during laser irradiation.

The polarization optical (top views) and scanning confocal laser micrographs for Glass A obtained by heat-assisted (250 °C) Nd:YAG laser irradiations with a laser power of $P = 1$ W and scanning speeds of $S = 0.5$ and 20 μm/s are shown in Figs. 4 and 5. In the present study, three-dimensional surface morphologies were obtained through successive piling up of color shades for two-dimensional slices. In both cases (Figs. 4 and 5), the change in the structure is observed. In the case of $S = 0.5$ μm/s, the morphology of the laser-irradiated surface is not smooth,

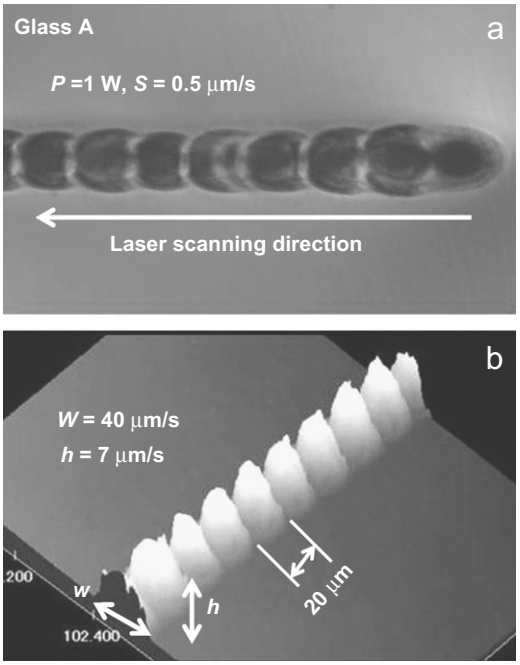

Fig. 4. Polarization optical (a) and confocal scanning laser (b) micrographs for the sample obtained by heat-assisted (250 °C) Nd:YAG laser irradiations with a laser power of $P = 1$ W and laser scanning speed of $S = 0.5$ μm/s in Glass A.

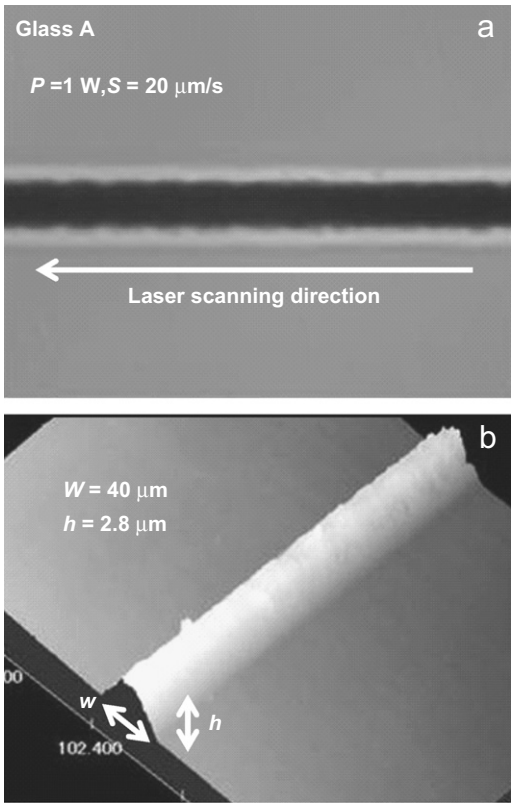

Fig. 5. Polarization optical (a) and confocal scanning laser (b) micrographs for the sample obtained by heat-assisted (250 °C) Nd:YAG laser irradiations with a laser power of $P = 1$ W and laser scanning speed of $S = 20$ μm/s in Glass A.

but periodic bumps like a backbone structure are observed along the laser scanning direction. Contrary, in the case of $S = 20$ μm/s, a more homogeneous surface structure, i.e., a bump with a width of 40 μm and a height of 2.8 μm, is observed. The data for the samples obtained by Nd:YAG laser irradiations with a laser power of $P = 1$ W and scanning speeds of $S = 2$ and 10 μm/s are shown in Fig. 6, indicating a gradual change in the bump morphology. It is clear from Figs. 4–6 that the surface morphology of the laser-irradiated region depends on laser scanning speed and changes from bump structures to homogeneous line structures with increasing laser scanning speed under the fixed laser power of $P = 1$ W.

In order to identify the structure of the laser-irradiated region, 100 lines were patterned in Glass A by scanning Nd:YAG laser with $P = 1$ W and $S = 20$ μm/s, in which the line patterning method and the sample size are shown in Fig. 7 schematically. The XRD pattern for such a laser-irradiated sample with 100 lines is shown in Fig. 8. The peaks are assigned to ferroelectric $Sr_xBa_{1-x}Nb_2O_6$ crystals with the ratio of Sr/Ba = 1 (JCPDS 39-0265), indicating that the lines obtained by Nd:YAG laser irradiations consist of SBN crystals being close to $Sr_{0.5}Ba_{0.5}Nb_2O_6$. The XRD pattern shown in Fig. 8, however, suggests that SBN crystals in the lines are formed randomly along the laser scanning direction, because all kinds of peaks are detected.

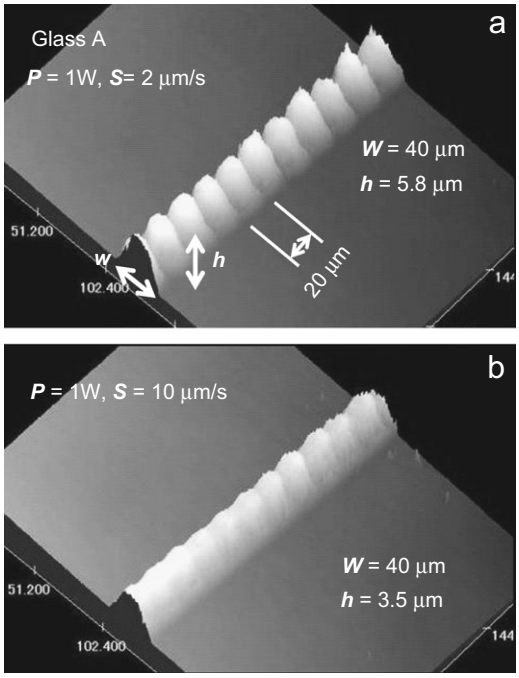

Fig. 6. Confocal scanning laser micrographs for the sample obtained by heat-assisted (250 °C) Nd:YAG laser irradiations in Glass A: (a) a laser power $P = 1$ W and laser scanning speed $S = 2\,\mu$m/s and (b) $P = 1$ W and $S = 10\,\mu$m/s.

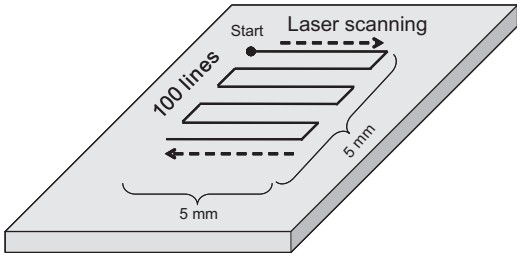

Fig. 7. Schematic illustration for the writing of 100 (Sr,Ba)Nb_2O_6 crystal lines on the glass surface by Nd:YAG laser irradiations.

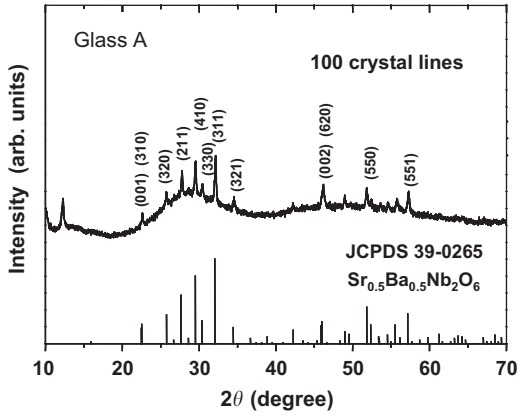

Fig. 8. XRD pattern for the assemblage of 100 lines written by heat-assisted (250 °C) Nd:YAG laser irradiations in Glass A. All peaks are assigned to $Sr_{0.5}Ba_{0.5}Nb_2O_6$ crystals.

As indicated in the above, the irradiation of Nd:YAG laser induces the crystallization of SBN crystals in Glass A. We also checked the feature of SBN crystals in the lines from polarized micro-Raman scattering spectroscopy. In measurements of polarized Raman scattering spectra, various configurations about the relationship between the direction of linearly polarized incident laser and the direction of linearly polarized Raman scattering light are possible, and an example is shown in Fig. 9. In this study, we measured polarized micro-Raman scattering spectra for two typical configurations against SBN crystals in the lines, i.e., $y(xx)\bar{y}$ and $y(zz)\bar{y}$. The results for the sample (Glass A) obtained by Nd:YAG laser irradiations with $P = 1$ W and $S = 20\,\mu$m/s are shown in Fig. 10. Two broad peaks with strong intensities are observed at 280 and 640 cm^{-1}. A broad peak with a small intensity is detected at 845 cm^{-1}, and a peak is present at 710 cm^{-1}. As can be seen in Fig. 10, the polarized Raman scattering spectra for both configurations of $y(xx)\bar{y}$ and $y(zz)\bar{y}$ are almost the same in the peak position and peak intensity. Almost similar polarized micro-Raman scattering spectra were observed for the line patterned by Nd:YAG laser irradiations with $P = 1$ W and $S = 0.5\,\mu$m/s.

The Raman scattering spectra for $Sr_xBa_{1-x}Nb_2O_6$ crystals have been reported by several researchers [28–31]. It is known that SBN crystal has significant intrinsic disorders in atomic arrangements, giving relaxor-type phase transitions and broad Raman scattering spectra in SBN crystals [28–31]. The bands at ~250, ~640, and 830 cm^{-1} are associated to the O–Nb–O bending, the Nb–O stretching, and a deformation of the NbO_6 octahedron, respectively [28–31]. The Raman scattering spectra shown in Fig. 10, therefore, demonstrate that the line patterned by Nd:YAG laser irradiations with $P = 1$ W and $S = 20\,\mu$m/s consists of SBN crystals. The peak located at 710 cm^{-1} in Fig. 10 has not been observed in SBN single crystals and will be associated to the Nb–O bond vibration (A1g mode) in $SrNb_2O_6$ or $BaNb_2O_6$ crystals [30]. It is, therefore, considered that the line patterned by Nd:YAG laser irradiations in Glass A includes not only SBN crystals but also $SrNb_2O_6$ or $BaNb_2O_6$ crystals.

As indicated above, although the lines with SBN crystals are formed in Glass A by Nd:YAG laser irradiations, the orientation of SBN crystals has not been confirmed and the impurity phase of $SrNb_2O_6$ or $BaNb_2O_6$ crystals is present. We tried to write homogeneous crystal lines consisting of only SBN crystals in other glasses, i.e., in Glass B and Glass C. The line was patterned in Glass B ($2NiO$–$4Bi_2O_3$–$16SrO$–$16BaO$–$32Nb_2O_5$–$30B_2O_3$) by heat-assisted (250 °C) Nd:YAG laser irradiations ($P = 1.0$ W, $S = 10\,\mu$m/s). And, the data on polarized optical micrograph, confocal scanning laser micrograph and polarized micro-Raman scattering spectra are shown in Figs. 11 and 12, respectively. The line with a smooth surface was obtained, and the formation of SBN crystals is confirmed from Raman scattering spectra. In particular, it should be pointed out that there is no peak at ~710 cm^{-1} in Raman

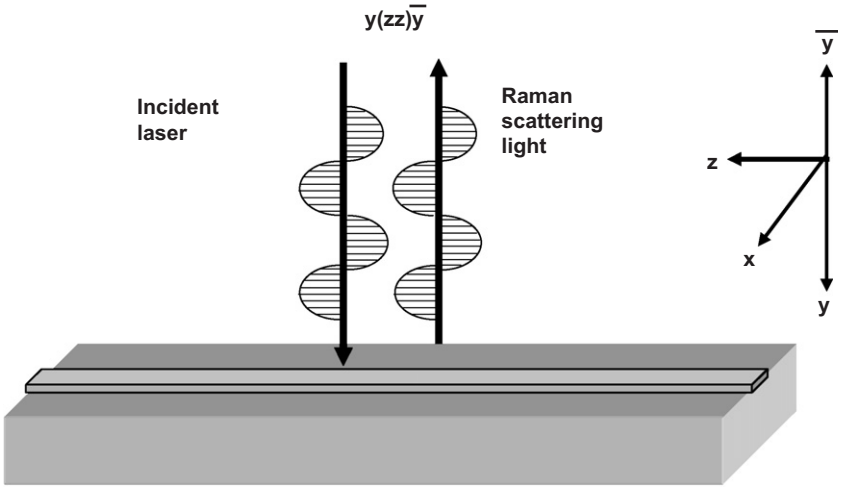

Fig. 9. Relationship between the direction of linearly polarized incident laser and the direction of linearly polarized Raman scattering light in the polarized micro-Raman scattering measurements.

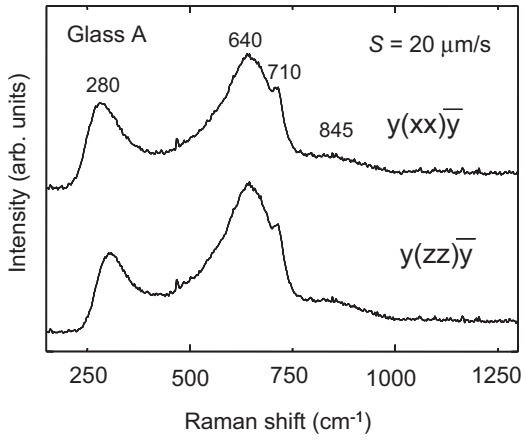

Fig. 10. Linearly polarized Raman scattering spectra for the line obtained by heat-assisted (250 °C) Nd:YAG laser irradiations with a laser power of $P = 1$ W and laser scanning speed of $S = 20$ μm/s in Glass A.

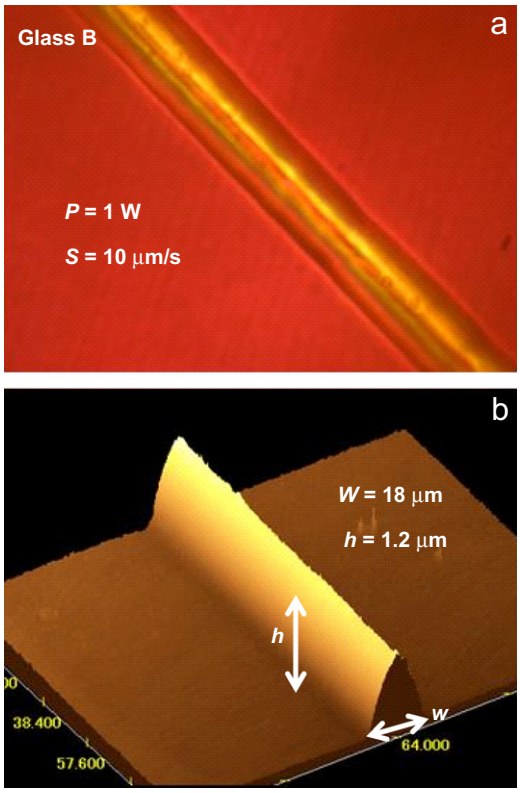

Fig. 11. Polarization optical (a) and confocal scanning laser (b) micrographs for the sample obtained by heat-assisted (250 °C) Nd:YAG laser irradiations with a laser power of $P = 1$ W and laser scanning speed of $S = 10$ μm/s in Glass B.

scattering spectra, suggesting that the line consists of only SBN crystals.

The lines consisting of SBN crystals were also patterned successfully in Glass C ($2NiO–4La_2O_3–16SrO–16BaO–32Nb_2O_5–30B_2O_3$) by heat-assisted (300 °C) Nd:YAG laser irradiations ($P = 1.0$ W, $S = 1$ μm/s), and the data on polarized optical micrograph, confocal scanning laser micrograph and polarized micro-Raman scattering spectra are shown in Figs. 13 and 14, respectively. The line with a smooth surface was also observed in Glass C. Furthermore, it is noted that the peak intensities of polarized micro-Raman scattering spectra change largely depending on the configurations of $y(xx)\bar{y}$ and $y(zz)\bar{y}$. The polarized Raman scattering spectra for a $Sr_{0.6}Ba_{0.4}Nb_2O_6$ single crystal commercially available are shown in Fig. 15, where the spectra were taken against the (1 0 0) plane. It is seen that the peak intensities change largely depending on the configuration of measurements. In the polarized Raman scattering spectra against the (0 0 1) plane for the $Sr_{0.6}Ba_{0.4}Nb_2O_6$ single crystal (not shown here), the peak intensities for the configurations of $y(xx)\bar{y}$ and $y(zz)\bar{y}$ were almost the same. The data shown in Fig. 14, therefore, suggest that SBN crystals in the line patterned by heat-assisted (300 °C) Nd:YAG laser irradiations ($P = 1.0$ W, $S = 1$ μm/s) in Glass C might orientate, i.e., the possibility of c-axis orientations of SBN crystals along the line growth

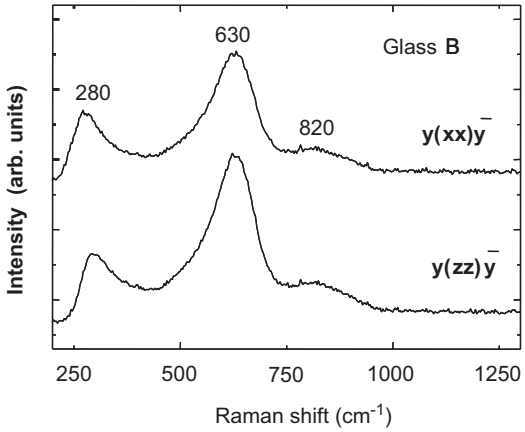

Fig. 12. Linearly polarized Raman scattering spectra for the line obtained by heat-assisted (250 °C) Nd:YAG laser irradiations with a laser power of $P = 1$ W and laser scanning speed of $S = 10\,\mu$m/s in Glass B.

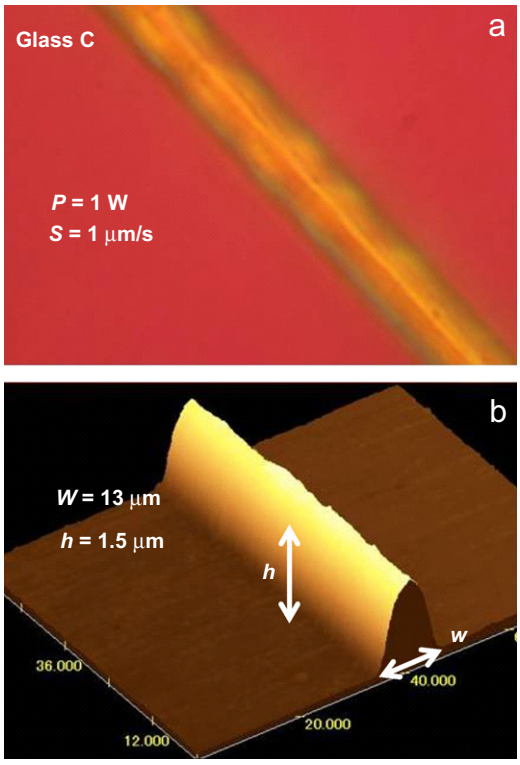

Fig. 13. Polarization optical (a) and confocal scanning laser (b) micrographs for the sample obtained by heat-assisted (300 °C) Nd:YAG laser irradiations with a laser power of $P = 1$ W and laser scanning speed of $S = 1\,\mu$m/s in Glass C.

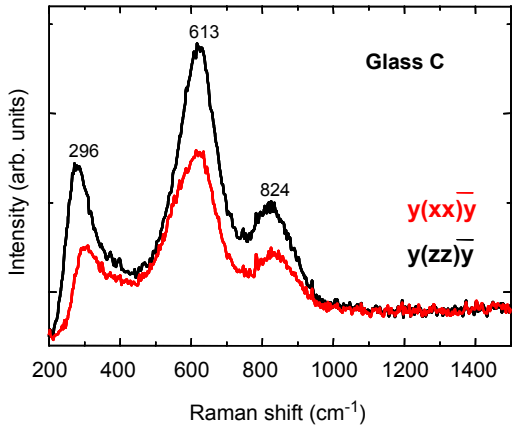

Fig. 14. Linearly polarized Raman scattering spectra for the line obtained by heat-assisted (300 °C) Nd:YAG laser irradiations with a laser power of $P = 1$ W and laser scanning speed of $S = 1\,\mu$m/s in Glass C.

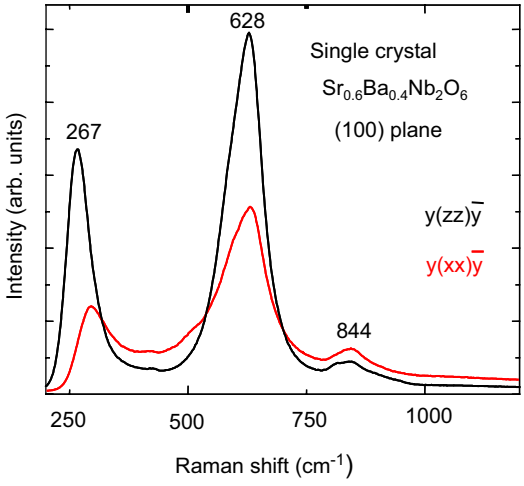

Fig. 15. Linearly polarized Raman scattering spectra for a $Sr_{0.6}Ba_{0.4}Nb_2O_6$ single crystal. The spectra were taken against the (1 0 0) plane.

direction (laser scanning direction). We have been trying to write a bumble (i.e., 100 lines) of SBN crystals lines in Glass C, but at this moment we cannot succeed to get such a sample because of the difficulty of constant writing of SBN crystal lines and thus do not have any XRD data for the SBN lines in Glass C. The crystallization temperature of Glass C is 723 °C, and this high crystallization temperature might be one of the reasons for the difficulty of constant writing of SBN crystal lines in our laser-induced crystallization technique. It is desired to write SBN crystal lines in other glasses with higher NiO contents (>3 mol%). In such glasses, it is expected that the temperature of Nd:YAG laser-irradiated region would be higher, inducing the crystallization of SBN crystals more easily.

3.3. Mechanism of laser-induced crystallization

The present study demonstrates that the combination of Ni^{2+} ion doping and cw Nd:YAG laser ($\lambda = 1064$ nm) irradiation, i.e., a TMAH processing, is working for the formation of SBN crystals on the surface of Bi_2O_3,-La_2O_3–SrO–BaO–Nb_2O_5–B_2O_3 glasses. The bump formation on the glass surface is one of the features in Nd:YAG laser-induced structural changes [19–22], indicating the volume expansion in the laser-irradiated region and suggesting the formation of low viscous super-cooled

liquid. Atomic rearrangements in glass occur at temperatures above the glass transition temperature. As the NiO-doped glass developed in this study have the values of $T_g = 555$–$611\,^{\circ}C$ and $T_p = 638$–$723\,^{\circ}C$, the maximum temperature of laser-irradiated region would be at least higher than $560\,^{\circ}C$. As already discussed by Inoue et al. [32] and Bennett et al. [33,34], laser irradiation to glass results in the increase of fictive temperature, i.e., larger molar volume and lower density. Bennett et al. [33] observed a bump formation in CO_2 laser-irradiated silicate glasses. It is considered that crystallization would not occur in the whole laser-irradiated region, consequently remaining bump morphologies as observed in the present study. It is important to check directly the size and morphology of SBN crystals in the lines by transmission electron microscope observations and also to evaluate the volume percentage of SBN crystals in the lines, i.e., the ratio of crystals and glassy phase. Such studies are now under consideration.

Crystallization of glass proceeds through two steps of nucleation process and crystal growth process. In order to write homogeneous crystal lines with highly oriented crystals, nucleation at the crystal growth front must be avoided. That is, at least the laser-irradiated region must have temperatures corresponding to extremely low nucleation rates and fast crystal growth rates. Considering the heat balance between laser energy absorbed by Ni^{2+} ions and heat dissipation from the laser-irradiated region to the surrounding glass medium, the temperature of the laser-irradiated region would depend on the amount of Ni^{2+} ions in a given glass, laser power, laser scanning speed, specific heat and thermal conductivity of glass.

As shown in Figs. 4–6, in the case of SBN crystal patterning in Glass A, the laser irradiation condition of the laser power of $P = 1$ W and scanning speed of $S = 0.5\,\mu m/s$ is not optimal for homogeneous line patterning. The periodic bump formation might indicate a periodic nucleation during laser scanning. On the other hand, the laser irradiation with $P = 1$ W and $S = 20\,\mu m/s$ in Glass A induces a more homogeneous surface morphology. Furthermore, the homogeneous lines are obtained in Glass B and Glass C. The homogeneous surface morphologies suggest that the nucleation tendency during laser irradiation in Glass B and Glass C is small. It would be necessary to determine the temperature profile of laser-irradiated regions as a function of laser power and scanning speeds for these glasses in order to clarify the mechanism of bump formation. At the same time, we should emphasize that glass composition itself is also very important for the patterning of SBN crystal lines, because the change in the glass composition gives not only the change in the temperature dependence of nucleation and crystal growth rates but also nucleation and crystal growth rates themselves. In this point of view, a search of new glass compositions being optimal for SBN crystal line patterning will be desired.

4. Conclusions

Crystal lines with $Sr_{0.5}Ba_{0.5}Nb_2O_6$ (SBN) were patterned on the surface of NiO-doped Bi_2O_3,La_2O_3–SrO–BaO–Nb_2O_5–B_2O_3 glasses by heat-assisted (250–300 °C) laser irradiations of continuous-wave Nd:YAG laser (wavelength: 1064 nm), and the surface morphology and the quality of SBN crystal lines were examined from measurements of polarization optical micrographs, confocal scanning laser micrographs, and polarized micro-Raman scattering spectra. It was found that the surface morphology of SBN crystal lines changed from periodic bump structures to homogeneous structures, depending on laser scanning conditions. It was suggested that some SBN crystals in the lines in $2NiO$–$4La_2O_3$–16SrO–16BaO–32Nb_2O_5–$30B_2O_3$ glass are oriented. The present study demonstrates that the TMAH processing (i.e., a combination of cw Nd:YAG laser and Ni^{2+} ions) is a novel technique for spatially selected crystallization of SBN crystals in glass.

Acknowledgments

This work was supported from Ministry of Internal Affairs and Communications Strategic Information and Communications R&D Promotion Programs (SCOPE), Grant-in-Aid for Scientific Research from the Ministry of Education, Science, Sports, Culture and Technology, Japan, and by the 21st Century Center of Excellence (COE) Program in Nagaoka University of Technology.

References

[1] P.V. Lenzo, E.G. Spencer, A.A. Ballman, Appl. Phys. Lett. 11 (1967) 23.
[2] M.D. Ewbank, R.R. Neurgaonkar, W.K. Cory, J. Feinberg, J. Appl. Phys. 62 (1987) 374.
[3] M. Horowitz, A. Bekker, B. Fischer, Appl. Phys. Lett. 62 (1993) 2619.
[4] G.A. Rakuljio, A. Yarw, R.R. Neurgaonkar, Opt. Eng. 25 (1986) 121.
[5] G.H. Beall, L.R. Pinckney, J. Am. Ceram. Soc. 82 (1999) 5.
[6] R. Sakai, Y. Benino, T. Komatsu, Appl. Phys. Lett. 77 (2000) 2118.
[7] F. Torres, K. Narita, Y. Benino, T. Fujiwara, T. Komatsu, J. Appl. Phys. 94 (2003) 5265.
[8] Y. Takahashi, Y. Benino, T. Fujiwara, T. Komatsu, J. Appl. Phys. 95 (2004) 3503.
[9] J.J. Shyu, J.R. Wang, J. Am. Ceram. Soc. 83 (2000) 3135.
[10] A.R. Kortan, N. Kopylov, B.I. Greene, A.M. Glass, J. Mater. Res. 17 (2002) 1208.
[11] D. Du, X. Liu, G. Korn, J. Squier, G. Mourou, Appl. Phys. Lett. 64 (1994) 3071.
[12] K.M. Davis, K. Miura, N. Sugimoto, K. Hirao, Opt. Lett. 21 (1996) 1729.
[13] H. Ebendorff-Heidepriem, Opt. Mater. 25 (2004) 109.
[14] R. Sato, Y. Benino, T. Fujiwara, T. Komatsu, J. Non-Cryst. Solids 289 (2001) 228.
[15] T. Honma, Y. Benino, T. Fujiwara, T. Komatsu, R. Sato, Appl. Phys. Lett. 82 (2003) 892.
[16] T. Honma, Y. Benino, T. Fujiwara, T. Komatsu, R. Sato, Appl. Phys. Lett. 83 (2003) 2796.

[17] T. Honma, Y. Benino, T. Fujiwara, T. Komatsu, Appl. Phys. Lett. 88 (2006) 231105.
[18] N. Chayapiwut, T. Honma, Y. Benino, T. Fujiwara, T. Komatsu, J. Solid State Chem. 178 (2005) 3507.
[19] M. Abe, Y. Benino, T. Fujiwara, T. Komatsu, R. Sato, J. Appl. Phys. 97 (2005) 123516.
[20] R. Ihara, T. Honma, Y. Benino, T. Fujiwara, R. Sato, T. Komatsu, Solid State Commun. 136 (2005) 273.
[21] R. Ihara, Y. Benino, T. Fujiwara, T. Komatsu, Adv. Mater. Res. 11/12 (2006) 209.
[22] T. Komatsu, R. Ihara, T. Honma, Y. Benino, R. Sato, H.G. Kim, T. Fujiwara, J. Am. Ceram. Soc. 90 (2007) 699.
[23] P. Gupta, H. Jain, D.B. Williams, J. Toulouse, I. Veltchev, Opt. Mater. 29 (2006) 355.
[24] J.S. Berks, W.B. White, Phys. Chem. Glasses 7 (1966) 191.
[25] D. Möncke, D. Ehrt, Glastech. Ber. Glass Sci. Technol. 74 (2001) 199.
[26] F.H.A. Elbatal, M.M.I. Khalil, N. Nada, S.A. Desouky, Mater. Chem. Phys. 82 (2003) 375.
[27] G. Lakshminarayana, S. Buddhudu, Spectrochim. Acta A 63 (2006) 295.
[28] E. Amazallag, T.S. Chang, R.H. Pantell, R.S. Feigelson, J. Appl. Phys. 42 (1971) 3254.
[29] K.G. Bartlett, L.S. Wall, J. Appl. Phys. 44 (1973) 5192.
[30] S.G. Lu, C.L. Mak, K.H. Wong, J. Am. Ceram. Soc. 86 (2003) 1333.
[31] J.L.B. Faria, P.T.C. Freire, A.P. Ayala, F.E.A. Melo, J.M. Filho, C.W.A. Paschoal, I.A. Santos, J.A. Eiras, J. Raman Spectrosc. 34 (2003) 826.
[32] S. Inoue, A. Nukui, K. Yamamoto, T. Yano, S. Shibata, M. Yamane, T. Maeseto, Appl. Opt. 37 (1998) 48.
[33] T.D. Bennett, D.J. Krajnovich, L. Li, D. Wan, J. Appl. Phys. 84 (1998) 2897.
[34] T.D. Bennett, D.J. Krajnovich, L. Li, J. Appl. Phys. 85 (1999) 153.